# Diffusion MRI Registration Using Orientation Distribution Functions

Xiujuan Geng[1], Thomas J. Ross[1], Wang Zhan[2], Hong Gu[1], Yi-Ping Chao[3], Ching-Po Lin[4], Gary E. Christensen[5], Norbert Schuff[2], and Yihong Yang[1]

[1] National Institute on Drug Abuse, NIH
gengx@mail.nih.gov
[2] Department of Radiology, University of California, San Francisco
[3] Department of Electrical Engineering, National Taiwan University, Taiwan
[4] Institute of Neuroscience, National Yang-Ming University, Taiwan
[5] Department of Electrical and Computer Engineering, University of Iowa

**Abstract.** We propose a linear-elastic registration method to register diffusion-weighted MRI (DW-MRI) data sets by mapping their diffusion orientation distribution functions (ODFs). The ODFs were reconstructed using a q-ball imaging (QBI) technique to resolve intravoxel fiber crossing. The registration method is based on mapping the ODF maps represented by spherical harmonics which yield analytic solutions and reduce the computational complexity. ODF reorientation is required to maintain the consistency with transformed local fiber directions. The reorientation matrices are extracted from the local Jacobian and directly applied to the coefficients of spherical harmonics. The similarity cost of the registration is defined by the ODF shape distance calculated from the spherical harmonic coefficients. The transformation fields are regularized by linear elastic constraints. The proposed method was validated using both synthetic and real data sets. Experimental results show that the elastic registration improved the affine alignment by further reducing the ODF shape difference; reorientation during the registration produced registered ODF maps with more consistent principle directions compared to registrations without reorientation or simultaneous reorientation.

## 1 Introduction

Diffusion-weighted magnetic resonance imaging (DW-MRI) is an emerging technique and plays an important role in studying white matter structure and anatomical connectivity. Non-rigid registration of DW-MRI images is crucial for building a white matter and fiber tract atlas and group analysis. With the assumption of a Gaussian diffusion profile, the second order diffusion tensor MRI (DTI) [1] provides a relatively simple approach for quantifying diffusion anisotropy as well as extracting local fiber directions. DTI Registration [2,3,4] has been studied and utilized in brain MRI analyses and produces additional information compared to conventional imaging modalities. However, a major drawback of DTI is that it fails to accurately characterize the diffusion in complex white matter, where fiber tracts with different orientations intersect within

J.L. Prince, D.L. Pham, and K.J. Myers (Eds.): IPMI 2009, LNCS 5636, pp. 626–637, 2009.

a voxel. Extension of DTI to higher orders [5] and multi-tensor models of the diffusivity profiles were recently introduced to solve this limitation. Another approach is q-space imaging (QSI) [6] which measures the diffusion function directly by employing the Fourier relation between the diffusion signal and the diffusion function. Due to the sampling burden and large pulse gradient requirements, q-ball imaging (QBI) techniques [7] haven been proposed, which sample the diffusion signals on a spherical shell and apply the Funk-Radon transform to reconstruct the model-free diffusion orientation distribution function (ODF) based on radial basis functions or spherical harmonics [8]. Spherical harmonics lead to an analytic solution for the ODF reconstruction and are widely utilized in various applications, such as shape modeling in molecular sciences and real-time lighting in computer graphics.

In this work we present a novel registration method for ODF maps represented by spherical harmonics. The potential of the ODF-based registration techniques is to align structures accordingly in locations where other image modalities are unable to characterize, for example, fiber crossings. However, the proposed technique is not restricted to ODF registration, it can also be applied to align the apparent diffusion profiles represented by spherical harmonics.

The registration is based on optimizing a cost function including the ODF shape similarity cost defined with a $L^2$ norm and an elastic regularization constraint. During the optimization, a rotation matrix is extracted at each voxel from the local Jacobian and converted to a general spherical harmonic rotation matrix to reorient the ODFs. The reorientation is directly applied to the coefficients without detecting principle directions ODFs which may have multiple directions and involve significant computation. We demonstrated the reorientation using both synthetic and real data sets. Experimental results show that the proposed registration method provides better performance in terms of smaller ODF shape difference and more consistent principle directions of the registered images, compared to registration without or with reorientation after registration.

## 2 Method

### 2.1 Diffusion ODFs Represented as Spherical Harmonics

The ODF characterizes the relative likelihood of water diffusion along any given angular direction $\mathbf{u}$ with $\mathbf{u}(\theta, \phi) = [\sin\theta\cos\phi \ \sin\theta\sin\phi \ \cos\theta]$ where $\theta$ and $\phi$ are the polar and azimuthal angles. Our registration method is applied to the reconstructed ODF maps from the QBI technique proposed by Hess *et al.* [8]. The ODF is approximated by a great circle integration on the sphere, i.e., $F(\mathbf{u}) = \oint_{\mathbf{q}\perp\mathbf{u}} E(\mathbf{q})d\mathbf{q}$. $E(\mathbf{q})$ represents an underlying diffusion-attenuated signal at a finite set of points on a sphere and $\mathbf{q}$ is the wavevector which describes diffusion encoding in a pulsed-gradient spin-echo experiment. The software "Camino" [9] is used to calculate and visualize ODFs.

As a single-valued spherical function, the function $F(\mathbf{u}) : S^2 \rightarrow R^+$, can be represented as a linear combination of a set of spherical harmonic basis $Y_l^m(\mathbf{u})$

with order $l$ and phase factor $m$: $F(\mathbf{u}) = \sum_{l=0}^{L} \sum_{m=-l}^{l} y_l^m Y_l^m(\mathbf{u})$, where $y_l^m$ denotes the harmonic series coefficient, and $L$ is the maximum harmonic order. Since $F$ is real, it is sufficient to utilize a real basis function set $Y_{lm}$, expanded as linear combinations of the complex harmonics:

$$Y_{lm}(\mathbf{u}) = \begin{cases} Y_l^0(\mathbf{u}) & , \text{ if } m = 0, \\ \frac{1}{\sqrt{2}}(Y_l^m(\mathbf{u}) + (-1)^m Y_l^{-m}(\mathbf{u})) & , \text{ if } m > 0, \\ \frac{i}{\sqrt{2}}((-1)^m Y_l^m(\mathbf{u}) - Y_l^{-m}(\mathbf{u})) & , \text{ if } m < 0. \end{cases} \tag{1}$$

$F$ is also assumed to be antipodal symmetric, such that the order $l$ only takes even numbers and the function can be expressed as

$$F(\mathbf{u}) = \sum_{l=0,\ \text{even}}^{L} \sum_{m=-l}^{l} c_m^l Y_{lm}(\mathbf{u}), \tag{2}$$

where $c_m^l$ represents the real harmonic series coefficient. In general, ODFs form an open subset of the space of complex-valued $L^2$ spherical functions with the induced $L^2$ norm $||F|| = \sqrt{< F, F >}$ [10]. In this work, we define the ODF shape difference with the $L^2$ norm. Other metrics, such as the Kullback-Leibler Divergence introduced by Chiang *et al.* [11], can also be applied to define the shape similarity. Given that the ODFs are represented with a complete set of orthonormal basis functions, they thus form a vector space analogue to unit basis vectors. The invariant shape norm and the distance between two functions can be defined as

$$||F|| = \sqrt{< F, F >} = \sqrt{\sum_{l=0,\text{even}}^{L} \sum_{m=-l}^{l} ||c_m^l||^2} \quad \text{and} \tag{3}$$

$$D(F_1, F_2) = ||F_1 - F_2|| = \sqrt{\sum_{l=0,\text{even}}^{L} \sum_{m=-l}^{l} ||c_{1m}^l - c_{2m}^l||^2}. \tag{4}$$

### 2.2 Rotation of Real Spherical Harmonics

A $3D$ rotation can be decomposed to three Euler angles using the $zyz$ convention with three subsequent rotations around the $z$, $y$ and $z$ axes by angles $\alpha_1$, $\alpha_2$ and $\alpha_3$, respectively: $\mathbf{R} = \mathbf{R}_Z(\alpha_3)\mathbf{R}_Y(\alpha_2)\mathbf{R}_Z(\alpha_1)$.

The coefficients of real spherical harmonics can be rotated in the same way as vectors with so-called Wigner matrices [12]. The coefficients $\lambda_m^l$ for the rotated function $\mathbf{R}(F(\mathbf{u})) = \sum_l \sum_m \lambda_m^l Y_{lm}(\mathbf{u})$ can be represented as a linear transformation of the original coefficients:

$$\lambda_m^l(\alpha_1, \alpha_2, \alpha_3) = \sum_{m'=-l}^{l} R_{mm'}^l(\alpha_1, \alpha_2, \alpha_3) c_{m'}^l. \tag{5}$$

The Wigner matrix $\mathbf{R}$ can be represented as a sparse block matrix:

$$\mathbf{R} = \begin{bmatrix} 1 & \mathbf{0} & \mathbf{0} & \cdots \\ \mathbf{0} & \mathbf{R^1} & \mathbf{0} & \cdots \\ \mathbf{0} & \mathbf{0} & \mathbf{R^2} & \cdots \\ \vdots & \vdots & \vdots & \ddots \end{bmatrix} \tag{6}$$

where $\mathbf{R}^l$ corresponds to the $l$-order. For complex spherical harmonics, a rotation operator expressed in terms of the Euler angle parametrization can be represented with a Wigner matrix with the matrix elements given by

$$D^l_{m'm}(\alpha_1, \alpha_2, \alpha_3) = e^{-im'\alpha_1} d^l_{m'm}(\alpha_2) e^{-im\alpha_3}, \quad \text{where} \tag{7}$$

$$\begin{aligned} d^l_{m'm}(\alpha_2) = & [\tfrac{(l+m')!(l-m')!}{(l+m)!(l-m)!}]^{1/2} \\ & \times \sum_{k=\max(0,m-m')}^{\min(l-m',l+m)} [(-1)^{k+m'-m} \tbinom{l+m}{k} \times \tbinom{l-m}{l-m'-k} \\ & \times (\cos\alpha_2/2)^{2l+m-m'-2k} (\sin\alpha_2/2)^{2k+m'-m}] \end{aligned} \tag{8}$$

Re-define the linear combination in Eq.(1) as $y_{lm}(\mathbf{u}) = \sum_{m'} A^l_{mm'} Y^l_{m'}(\mathbf{u})$, then the rotation matrix for real spherical harmonics is given by

$$\mathbf{R}^l = A^l D^l A^{l\dagger}, \tag{9}$$

where † is the complex conjugate transpose. The $z$-axis rotation of spherical harmonics is straightforward and can be calculated as follows, without constructing $\mathbf{R}_Z$:

$$\lambda^l_m = c^l_{-m} \sin(-m\alpha) + c^l_m \cos(m\alpha). \tag{10}$$

To implement $\mathbf{R}_Y$, we followed Eq.(20) in [13]. A fast spherical harmonic rotation approximation using a truncated Taylor expansion of $\mathbf{R}_Z$ [14] can be used to speed up the calculation, however the accuracy is compromised.

### 2.3 Reorientation of Diffusion ODFs

Image registration searches for transformations to map structures in the source to corresponding ones in the reference. By assumption, the water diffusion orientation distributions reflect the underlying fiber structures; therefore, ODF reorientation along the transformation is required. The Jacobian of the spatial transformations is the first order linear approximation to the differentiable functions at a given spatial location. Therefore, a natural thought is to apply the Jacobian to the ODF at each location to reorient it. Using this strategy, the shape and size of the ODFs are subject to change. To keep the shape invariant, we apply the rotation matrix extracted from the Jacobian to reorient the ODFs, which is similar to the "finite strain" tensor reorientation technique proposed by Alexander *et al.* [2]. Since a diffusion ODF may have multiple local maxima indicating multiple crossing fibers, which are computationally expensive to detect, direct implementation of the "preservation of principal directions

(PPD)" method [2] may not work efficiently. A convenience of formulating ODFs with spherical harmonics is that the shape rotation can be achieved by apply a rotation matrix directly to the coefficients (see Sec.2.2) without changing of the basis functions and without reconstruction of the ODFs after reorientation during each registration step. The invariance of the basis functions simplifies the calculation of the shape difference which can be always preformed using the corresponding coefficients as described in Eq.(4).

Chiang *et al.* [11] proposed a reorientation method that first detected the principle direction of the diffusivity functions by shape-based PCA, and then applied PPD to reorient the diffusivity function. A major difference of our approach is that, instead of computing the diffusion attenuation signal at each reoriented direction, we apply the rotation matrices directly to the coefficients to get the reoriented ODF. As QBI techniques normally acquire several hundred sampling directions, performing operations on much fewer coefficients reduces the computation cost significantly. Barmpoutis *et al.* [5] noted limitations of the re-orientation of diffusivity functions, and provided a full affine "re-transform" of diffusion functions instead of reorientation under a 4th order tensor model.

### 2.4 Registration of ODFs

The ODF-based registration can be stated as an optimization problem of finding spatial transformation $h_{12}$ that minimizes the following cost function:

$$\begin{aligned} C &= C_{SIM} + C_{REG} \\ &= \sigma \int_{\Omega} ||D(\mathbf{R}_{12}(F_1(h_{12}(x))), F_2(x))||^2 dx + \rho \int_{\Omega} ||\mathcal{L}(u_{12}(x))||^2 dx \\ &= \sigma \int_{\Omega} \sum_{l=0,even}^{L} \sum_{m=-l}^{l} ||\lambda_{1m}^{l}(h_{12}(x)) - c_{2m}^{l}(x)||^2 dx \\ &+ \rho \int_{\Omega} ||\nabla^2(u_{12}(x))||^2 dx \end{aligned} \tag{11}$$

where $\Omega$ represents the ODF map space, $\sigma$ and $\rho$ are weighting parameters for the similarity and regularization costs, respectively, $\mathbf{R}_{12}$ is the associated reorientation matrix of the ODF $F_1$ at $h_{12}(x)$, $\lambda_m^l$ is the rotated coefficient defined in Eq.(5), and $u_{12}(x)$ is the displacements satisfying $h_{12}(x) = x + u_{12}(x)$. The similarity term was defined using the shape difference metric in Eq.4. $\mathcal{L}$ is a linear differential operator and was defined to be the Laplacian operator in this work, i.e., $\mathcal{L} = \nabla^2 = \left[\frac{\partial^2}{\partial x_1^2} + \frac{\partial^2}{\partial x_2^2} + \frac{\partial^2}{\partial x_3^2}\right]$. The transformations were initialized as identities, and updated by gradient descent iteratively. At each iteration, linear interpolation of the reoriented coefficients $\lambda_m^l$ was used to generate the deformed ODF maps.

The transformation fields are defined in Eulerian space, therefore the reorientation matrix operating on the deforming ODF should be extracted from the inverse of $J(h_{12})$ with the following equation

$$\mathbf{R}_{12} = ((J(h_{12}) \cdot J(h_{12})^T)^{-\frac{1}{2}} J(h_{12}))^T. \tag{12}$$

To apply the rotation to the spherical harmonic coefficients, $\mathbf{R}_{12}$ is decomposed into three Euler angles using the $zyz$ convention. Let $c_1$ denote $cos(\alpha_1)$, $s_1$ denote $sin(\alpha_1)$, and define $c_2$, $s_2$, $c_3$ and $s_3$ accordingly. Then $\mathbf{R}(\alpha_1\alpha_2\alpha_3)$ is expressed as:

$$\begin{bmatrix} c_1c_2c_3 - s_1s_3 & -c_2c_3s_1 - c_1s_3 & c_3s_2 \\ c_3s_1 + c_1c_2s_3 & c_1c_3 - c_2s_1s_3 & s_2s_3 \\ -c_1s_2 & s_1s_2 & c_2 \end{bmatrix} \tag{13}$$

Therefore, the three Euler angles can be obtained as:

$$\alpha_1 = -\arctan(R_{32}, R_{31}),\ \alpha_2 = \arccos(R_{33}),\ \text{and}\ \alpha_3 = \arctan(R_{23}, R_{13}), \tag{14}$$

with the constraints of $\alpha_1 \in [-\pi\ \pi]$, $\alpha_2 \in [-\frac{\pi}{2}\ \frac{\pi}{2}]$, and $\alpha_3\ \in [-\pi\ \pi]$. $R_{ij}$ represents the element of $\mathbf{R}$ in the $i$th row and $j$th column, and $(R_{ij}, R_{kl})$ represents the angle vector coordinate in the plane. Note that $\arctan(a, b)$ is almost equivalent to $\arctan(a/b)$ except that we also take into account the quadrant in which the point (a,b) is located.

## 3 Experiments and Results

### 3.1 Synthetic Experiments of Reorientation

Diffusion tensors with three mixtured zero-mean Gaussians under low intravoxel water exchange model were simulated with SNR of 100 using "Camino". The largest eigenvalues of the three tensors were set to be $3\times10^{-9}m^2/s$, $2\times10^{-9}m^2/s$ and $1.5 \times 10^{-9}m^2/s$ along the x, y and z axes, respectively. The other two eigenvalues had a value of $0.6 \times 10^{-9}m^2/s$ along the $y$ and $z$ axes, the $x$ and $z$ axes, and the $x$ and $y$ axes. 162 encoding directions were used for the QBI acquisition with $b = 3000\ s/mm^2$. Fig. 1 (a) shows the reconstructed ODF projected on the $xy$ and the $xz$ planes. 30° rotations along the $z$-axis and along $y$-axis were applied separately on the spherical harmonic coefficients according to Eq.(9), (7), (8) and (10). The reconstructed ODF are shown in Fig. 1 (b) and (c). Fig. 1 (d) plots the coefficients of the original and rotated ODFs. Fig.2 demonstrates a spatial rotation of 25° of a real DW-MRI data set without and with ODF reorientation. A rotation transformation without ODF reorientation resulted in an inconsistency between the principle directions of the ODFs and the underlying fiber directions. With ODF reorientation of the coefficients, the principle directions were rotated to follow the transformed fiber structures.

### 3.2 Registration Experiments with Real Data

Human brain QBI data from five healthy subjects were acquired on a 3T TrioTim Siemens MRI scanner. Isotropic axial diffusion-weighted images were obtained using a single shot diffusion spin-echo echo-planar imaging (EPI) sequence with TR/TE = 9,500/116 ms, FOV= 192 mm, matrix size = 96×96, yielding a 2mm image resolution. 162 diffusion encoding directions (using an electrostatic repulsion model) with a $b$ value of 3000 s/mm$^2$ and one reference image with $b = 0$

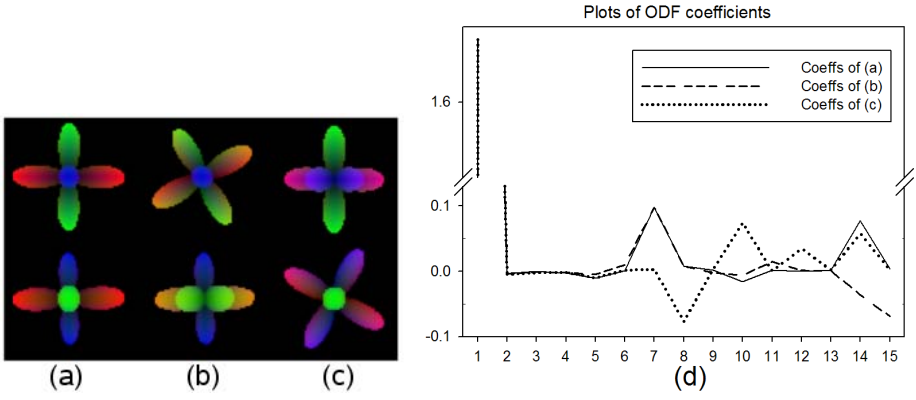


**Fig. 1.** Illustration of the ODF reorientation with simulated 3-tensor data sets. (a) the original ODF projected on the $xy$ plane on the top and the $xz$ plane at the bottom; (b) the ODF rotated 30° along the $z$-axis; (c) the ODF rotated 30° along the $y$-axis; and (d) the plots of corresponding ODF coefficients stored in a $1d$ array $[c_0^0, c_{-2}^2, c_{-1}^2 \cdots, c_3^4, c_4^4]$.

were acquired. 60 slices with slice thickness of 2mm were obtained to cover the whole brain. The total scan time was 25.65 minutes.

ODF maps of each data set were reconstructed with real spherical harmonics following the technique in [8]. The maximum harmonic order was set to 4 in this preliminary study resulting in $(4+1) \times (4+2)/2 = 15$ coefficients to represent the diffusion functions. The proposed method is general to any order of spherical harmonics. One data set was selected as the reference and the other four were registered to it. The mean shape of the ODF at each voxel location was calculated following Eq.(4) and used to perform the scalar-based affine registration. The affine matrices were then decomposed to Euler rotation angles using Eq.(12) and Eq.(14) and applied to transform the coefficients to reorient the ODFs. The affine aligned images were regarded as inputs to register to the reference using the elastic registration described in Sec.2.4. The parameters were set to: the similarity weight $\sigma = 1$, the regularization weight $\rho = 0.4$, and the number of iterations = 100. A Gaussian filter with $FWHM = 1.77mm$ was applied to smooth the deformation fields at each iteration. The similarity error converged after around 50 iterations for all registrations.

To demonstrate the contribution of the ODF reorientation, the experiments were designed to compare the proposed method with reorientation at each iteration to registration methods without reorientation, and with reorientation after registration. All three methods used the same registration parameters.

Two metrics were computed for evaluation and comparison: the average of ODF shape difference defined in Eq.(4) and the average directional consistency of the largest principle direction of the registered ODF maps. The average directional consistency is defined as $adc = \frac{1}{N}\sum_i |\mathbf{u}_1(i) \cdot \mathbf{u}_2(i))|$, where $\mathbf{u}_1$ is the

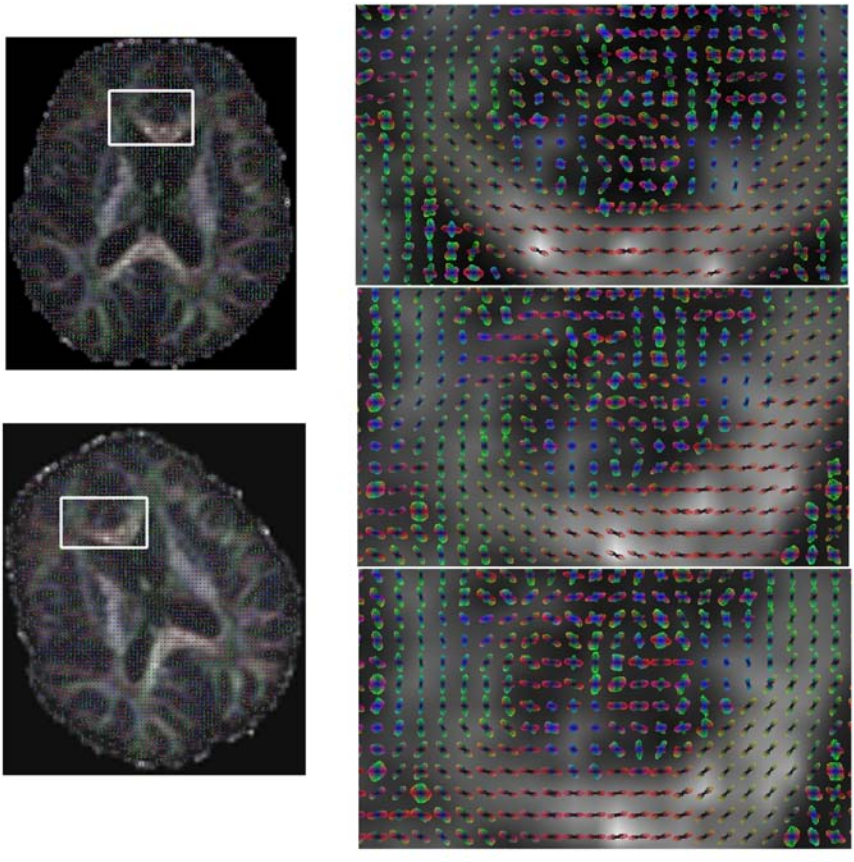

**Fig. 2.** Illustration of ODF reorientation using real qball imaging (QBI) data with a 25° rotation along the $z$-axis. The underlays are the fractional anisotropy (FA) maps calculated by a single tensor model. The overlays are reconstructed ODFs using QBI. The enlarged figures on the right from top to bottom are: original ODFs on the original FA image; ODFs without reorientation on the rotated FA image; and ODFs with reorientation on the rotated FA image.

largest principle direction of the deformed ODF map at voxel $i$, $\mathbf{u}_2$ is the largest principle direction of the reference ODF map at voxel $i$ and $N$ is the number of voxels where both deformed and reference maps have nonzero values. The closer to 1 that the measure is, the more consistent the largest principle directions between the deformed and the reference map are. The reason for taking the absolute value of the dot product is due to the assumption of antipodal symmetry of the ODFs. The peak direction was calculated by searching the local maximum within a fixed search radius of 0.4 and randomly rotating a unit icosahedron 8672 times using "Camino".

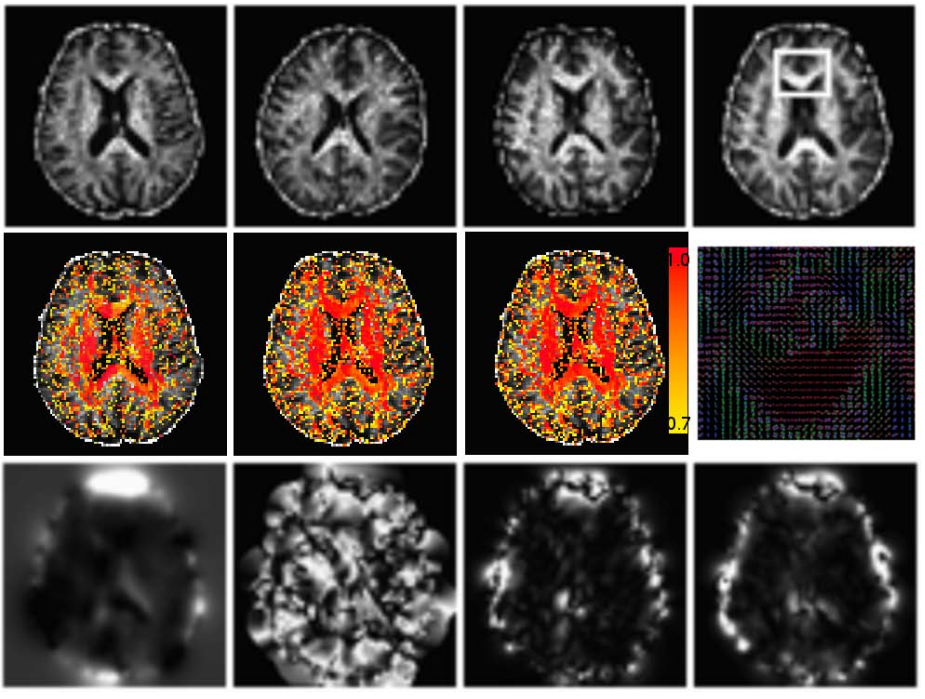


**Fig. 3.** Typical ODF registration results with various registration methods. The top row from left to right: the mean shape of the ODF maps of the reference, source, source after affine alignment and after elastic registration with reorientation; the second row from left to right: directional consistency maps after affine registration with reorientation, elastic registration without reorientation and elastic registration with reorientation, and the enlarged ODFs of the boxed region in the above figure; the bottom row from left to right: the norm of the transformation fields, the rotation angle $\alpha_1$ along $z$-axis, $\alpha_2$ along $y$-axis and the sum of the first rotation angle $\alpha_1$ and second angle $\alpha_3$ along $z$-axis.

The mean shape of the ODF maps of the reference, original source, source after affine alignment and after elastic registration are shown in the top row of Fig.3. The alignment of brain structures is improved from affine to elastic registration around several regions such as the corpus callosum and the ventricles. Fig.3 also shows the enlarged ODFs after elastic registration with reorientation of the selected box region. We found that the ODF maps are smooth and follow the structural directions. The directional consistency maps after affine registration with reorientation, elastic registration without reorientation and elastic registration with reorientation are shown in the second row of Fig.3. The values are color-coded from 0.707 (corresponding to 45° angular difference) to 1. Larger values from affine to elastic registration are observed which indicate greater consistency of the direction peaks between the deformed and reference maps. The

**Table 1.** Registration results for the four subjects measured by average shape difference and directional consistency metrics. Affine without reorientation (ro) and with ro, elastic without ro, with ro after registration (roa) and with ro during registration methods were compared.

| | ave shape difference | | | | ave directional consistency | | | |
|---|---|---|---|---|---|---|---|---|
| method | 1 | 2 | 3 | 4 | 1 | 2 | 3 | 4 |
| affine wo/ro | 4.905 | 3.332 | 3.333 | 4.239 | 0.475 | 0.479 | 0.472 | 0.468 |
| affine w/ro | 4.900 | 3.320 | 3.331 | 4.220 | 0.481 | 0.483 | 0.504 | 0.480 |
| elastic wo/ro | 2.011 | 1.589 | 1.617 | 1.987 | 0.595 | 0.598 | 0.580 | 0.566 |
| elastic w/roa | 1.987 | 1.580 | 1.612 | 1.976 | 0.599 | 0.601 | 0.590 | 0.572 |
| elastic w/ro | 1.976 | 1.576 | 1.604 | 1.962 | 0.609 | 0.608 | 0.598 | 0.585 |

difference is subtle to be seen between with and without reorientation using elastic registration. Slightly greater values in the genu and splenium of the corpus callosum can be observed. The norm of the transformation fields, the rotation angle $\alpha_1$ along $z$-axis, $\alpha_2$ along $y$-axis and the sum of the first and second rotation angles $\alpha_1$ and $\alpha_3$ along $z$-axis are displayed in the bottom row of Fig.3. The composition of $\alpha_1$ and $\alpha_3$ play the major role in the rotation along the $z$-axis, given that the rotation angles along $y$-axis are small (which is the case in this experiment). Therefore the unsmooth $\alpha_1$ map does not imply the unsmooth rotation fields along the $z$-axis, but the sum of $\alpha_1$ and $\alpha_2$ gives an indication of the degree of smoothness of rotation fields along the $z$-axis. This can be seen by the fact that a first large rotation along the $z$-axis can be canceled out by a second large but negative direction rotation along $z$-axis. There are some places around the boundary that the rotation angle fields are not very smooth. A regularization term on the rotation fields may help to produce a smoother rotation.

Tab.1 shows the affine and elastic registration results with and without reorientation measured by the average shape difference and directional consistency metrics. In general, the elastic registration methods significantly reduced the ODF shape difference and improved directional consistency compared to the affine methods. The reorientation after affine alignment slightly improved the shape similarity and directional consistency. All elastic methods used the affine aligned ODF maps as inputs. Based on the four sets of registration results, reorientation after registration produced slightly better results compared to registration without reorientation, which demonstrates the need of reorienting ODFs to keep them consistent with the deformed local structures. Simultaneous reorientation further improved the performance in terms of smaller average shape difference and larger directional consistency, which shows that it has the potential to help the registration process to get out of local minima.

The small improvements of shape similarity caused by ODF reorientation may be due to the relatively insensitive shape metric under rotation. The shape difference metric used here includes the 0-order spherical harmonics which are invariant under rotation and take a large portion in the distance calculation ( see Fig.3 (d)). Metrics more sensitive to rotation, such as computing the difference

using all but the 0 order coefficients would potentially magnify the improvement. One reason of the small amount of improvement measured by the directional consistency metric is because it was averaged over the whole brain instead of in specific regions. Due to the relatively low SNR (around 10) in QBI data, in many gray matter regions, the ODF peaks may not truly reflect the underlying structures. The peaks in those regions between source and reference have large differences to begin with and are hard to match even with ODF reorientation. The calculation of the differential of the ODF reorientation is ignored in this work, and taking into account it may improve the registration performance [15].

## 4 Conclusions and Discussion

We presented a novel DW-MRI registration algorithm based on reconstructed ODFs represented by spherical harmonics. The ODF reorientation was performed during the elastic registration procedure. The reorientation matrices were obtained by extracting the rotation part from the local Jacobian and directly applied to the spherical harmonic coefficients to rotate the ODF. Computation of the principal directions and reconstruction of the ODFs during each registration iteration are avoided. The similarity cost was computed based on a shape difference metric defined using the $L^2$ norm. A linear elastic regularization term was added to constrain the transformation fields. ODF reorientation was tested using synthetic q-ball data and real q-ball data with known rotation angles. The registration method was evaluated and compared with affine registration and elastic registration without reorientation or with reorientation after registration. Average shape difference and directional consistency were measured and compared with various registration techniques. Results show that the elastic registration model significantly reduced ODF shape difference and improved directional consistency; simultaneous reorientation further improved the registration performance.

A limitation of the proposed ODF-based registration is that it fully depends on the quality of the reconstructed ODF maps. Metrics derived from other models (such as fractional anisotropy from DTI) or directly from diffusion attenuation signals (i.e., mean shape of the acquired signals instead of the reconstructed ones) may help to validate the registration performance and analyze how much the reconstructed ODF would affect the registration results. Other possible areas to improve the method include to apply the motion correction of the EPI data sets to get more accurate ODFs and therefore better registration; to use a multi-resolution registration scheme to avoid local minima; and to include the differential of ODF reorientation in the registration optimization procedure.

## Acknowledgments

This work was supported by the Intramural Research Program of the National Institute on Drug Abuse (NIDA), National Institute of Health (NIH).

## References


1. Basser, P.J., Pierpaoli, C.: Microstructural and physiological features of tissues elucidated by quantitative-diffusion-tensor MRI. Journal of Magnetic Resonance, Series B 111, 209–219 (1996)
2. Alexander, D., Pierpaoli, C., Basser, P., Gee, J.: Spatial transformations of diffusion tensor magnetic resonance images. IEEE Trans. Med. Imaging 20(11) (2001)
3. Verma, R., Khurd, P., Davatzikos, C.: On analyzing diffusion tensor images by identifying manifold structure using isomaps. IEEE Trans. Med. Imaging 26(6), 772–778 (2007)
4. Zhang, H., Avants, B.B., Yushkevich, P.A., Woo, J.H., Wang, S., McCluskey, L.F., Elman, L.B., Melhem, E.R., Gee, J.C.: High-dimensional spatial normalization of diffusion tensor images improves the detection of white matter differences: An example study using amyotrophic lateral sclerosis. IEEE Trans. Med. Imaging 26(11) (2007)
5. Barmpoutis, A., Jian, B., Vemuri, B.C., Shepherd, T.M.: Symmetric positive $4^{th}$ order tensors & their estimation from diffusion weighted MRI. In: Karssemeijer, N., Lelieveldt, B. (eds.) IPMI 2007. LNCS, vol. 4584, pp. 308–319. Springer, Heidelberg (2007)
6. Gilbert, R., Magnusson, L., Napadow, V., Benner, T., Wang, R., Wedeen, V.: Mapping complex myoarchitecture in the bovine tongue with diffusion- spectrum-magnetic resonance imaging. Biophys. 91, 1014–1022 (2006)
7. Tuch, D.S.: Q-ball imaging. Magnetic Resonance in Medicine 56, 1358–1372 (2004)
8. Hess, C., Mukherjee, P., Han, E., Xu, D., Vigneron, D.: Q-ball reconstruction of multimodal fiber orientations using the spherical harmonic basis. Magnetic Resonance in Medicine 56, 104–117 (2006)
9. Cook, P.A., Bai, Y., Nedjati-Gilani, S., Seunarine, K.K., Hall, M.G., Parker, G.J., Alexander, D.C.: Camino: Open-source diffusion-mri reconstruction and processing. In: 14th Scientific Meeting of the International Society for Magnetic Resonance in Medicine (2006)
10. Zhang, H., Yushkevich, P.A., Gee, J.C.: Registration of diffusion tensor images. In: 2004 Conference on Computer Vision and Pattern Recognition (CVPR 2004), pp. 842–847. IEEE Computer Society, Los Alamitos (2004)
11. Chiang, M., Klunder, A., McMahon, K., de Zubicaray, G., Wright, M., Toga, A., Thompson, P.: Information-theoretic analysis of brain white matter fiber orientation distribution functions. In: Karssemeijer, N., Lelieveldt, B. (eds.) IPMI 2007. LNCS, vol. 4584, pp. 172–182. Springer, Heidelberg (2007)
12. Edmonds, A.: Angular Momentum in Quantum Mechanic. Princeton University Press, Princeton (1996)
13. Ritchie, D.W., Kemp, G.J.L.: Fast computation, rotation, and comparison of low resolution spherical harmonic molecular surfaces. Journal of Computational Chemistry 20(4), 383–395 (1999)
14. Krivanek, J., Konttinen, J., Pattanaik, S., Bouatouch, K., Zara, J.: Fast approximation to spherical harmonic rotation. In: International Conference on Computer Graphics and Interactive Techniques (2006)
15. Yeo, B.T.T., Vercauteren, T., Fillard, P., Pennec, X., Golland, P., Ayache, N., Clatz, O.: Dti registration with exact finite-strain differential. In: Proceedings of the International Symposium on Biomedical Imaging (2008)